Dyes and Pigments 178 (2020) 108353

Contents lists available at ScienceDirect

Dyes and Pigments

journal homepage: http://www.elsevier.com/locate/dyepig

Synthesis and fluorescent studies of a low molecular weight rotor for living cancer cell imaging

Shulei Zhu [a], Xumeng Yu [a], Yang He [a], Mingliang Ma [a,b,**], Wei Lu [a,*]

[a] Shanghai Engineering Research Center of Molecular Therapeutics and New Drug Development, School of Chemistry and Molecular Engineering, East China Normal University, 3663 North Zhongshan Road, Shanghai, 200062, PR China

[b] Key Laboratory of Brain Functional Genomics-Ministry of Education, School of Life Science, East China Normal University, 3663 North Zhongshan Road, Shanghai, 200062, PR China

ARTICLE INFO

Keywords:
Fluorescence
Molecular rotor
Low molecular weight
Cancer cell imaging

ABSTRACT

A fluorescent and low molecular weight rotor (**9**) based on 1, 8-napthalimide for living cancer cell imaging was designed and synthesized. The effects of solvent polarity and viscosity on the fluorescence spectra of compound **9** were investigated. Rotor **9** exhibited favorable photophysical properties with a large Stokes shift and induced high viscosity sensitivity in a glycerol-ethanol system with an approximately 10-fold increase in emission intensity. The addition of different concentrations of BSA to compound **9** in PBS elicited an 8-fold increase in fluorescence intensity, suggesting superior environmental sensitivity. Fluorescence lifetime measurements also confirmed these results. Furthermore, compound **9** showed time- and concentration-dependent *in vitro* cellular uptake behavior in MCF-7 cells and other cancer cell lines. CLSM assay of tumor sections from MCF-7 nude mice also confirmed the possibility of tumor imaging.

1. Introduction

Fluorescent dyes are an important class of colorants due to their widespread application in paints, textiles, foodstuffs, fertilizers, and pharmaceuticals [1,2]. Their fluorescence properties are easily modulated through the implementation of various types of photophysical processes such as photoinduced electron transfer (PET) [3–5], intramolecular charge transfer (ICT) [6–8], aggregation-caused quenching (ACQ) [9] and aggregation-induced emission (AIE) [10–13]. Because of these properties, dyes are also widely used for potential applications in bio-imaging [14], fluorescent chemo/biosensors [15], organic light-emitting diodes (OLEDs), as well as other optical devices [16]. In particular, the use of fluorescent dyes in living systems has attracted a great deal of academic and industrial interest because they provide an excellent tool for detection, imaging, and diagnosis owing to their high spatial resolution, real-time analysis and low toxicity [17,18].

It is widely reported that fluorescent dyes are sensitive to an array of factors, such as ion concentration, rigidity, viscosity and biomolecule binding [19]. Environmentally sensitive fluorescent dyes by virtue of their sensitivity to various media provide a wealth of information on the chemical and physical properties that may affect their applications [20,21]. Among these factors, viscosity and protein binding played vital roles in different biological functions both at the cellular and organism levels [1,22–24]. Several groups have reported that the viscosity of the cell membrane can affect the active transportation of bioactive molecules through the membrane, which was linked with many diseases and disorders [18,25,26]. However, traditional mechanical methods for the quantitative measurement of intracellular micro-viscosity still faces challenges.

Fluorescent viscosity sensors are known as Fluorescent Molecular Rotors (FMRs), whose fluorescence intensity is affected by twisted intramolecular rotation that is dependent upon the viscosity of the surrounding environment [27,28]. Intramolecular charge transfer (ICT) is one of the key characteristics of FMRs containing the donor–π–acceptor (D-π-A) feature, which reduces the HOMO-LUMO band gap, leading to outstanding properties [29,30]. Many typical fluorescent sensors have been previously reported such as aniline nitriles [31], julolidine malononitriles [32] and stilbenes [31] (Fig. 1). It's difficult to firmly establish relationships between the molecular structure and viscosity sensitivity and thus there is a requirement to

* Corresponding author.
** Corresponding author. Shanghai Engineering Research Center of Molecular Therapeutics and New Drug Development, School of Chemistry and Molecular Engineering, East China Normal University, 3663 North Zhongshan Road, Shanghai, 200062, PR China.
E-mail addresses: mlma@brain.ecnu.edu.cn (M. Ma), wlu@chem.ecnu.edu.cn (W. Lu).

https://doi.org/10.1016/j.dyepig.2020.108353
Received 21 December 2019; Received in revised form 7 March 2020; Accepted 10 March 2020
Available online 14 March 2020

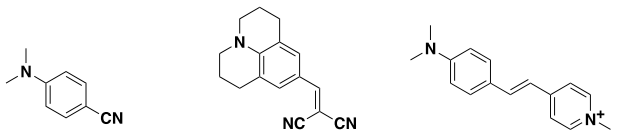

Fig. 1. The structures of typical fluorescent sensors including aniline nitriles (DMABN, **1**), julolidine malononitriles (DCVJ, **2**), and stilbenes (p-DASPMI, **3**).

rationally develop fluorescent sensors used to measure viscosity with high sensitivity, high spatial and temporal resolution in microenvironments.

In this work, we proposed to prepare an organic fluorescent viscosity sensor using the principle of ICT. Molecular rotor **9** (Scheme 1) was designed and synthesized with a phenol unit as an electron donor and a 1,8-naphthalimide as an electron acceptor [33–36]. Compared with many existing FMRs, the synthetic route is based on simple reactions and only five steps, which reduced the cost [37–41]. The naphthalimide was chosen as the fluorophore because of its high fluorescence efficiency and sufficient photostability. The photophysical and FMR properties in different polarity and viscosity solvents have been studied. Fluorescence lifetime further confirmed the photophysical and FMR properties, demonstrating high fluorescence contrast compared with existing FMRS [37–41]. In addition, *in vitro* cellular uptake against four cancer cell lines and the CLSM assay of MCF-7 nude mice tumor sections were also examined to demonstrate the possibility of **9**'s application in living cancer cell imaging.

2. Experimental section

2.1. Materials and instruments

PEG400 and Rhodamine 6G were obtained from Bidepharm. Bovine serum albumin (BSA) was purchased from Energy Chemical. The other reagents used were all spectroscopic grade. All solvents were degassed and sparged with argon prior to use. UV–visible (UV–Vis) absorption spectra and emission spectra and fluorescence spectra were determined at room temperature at concentrations around 1 μM with a Varian Cary 100 spectrophotometer and Hitachi F-4500 fluorescence spectrophotometer with slit widths routinely set at 2.5 nm, respectively. Fluorescence lifetime was recorded on the F-7000 fluorescence spectrometer (Hitachi, Japan). NMR spectra were recorded on a Bruker DRX-400 MHz spectrometer. Chemical shifts were reported in ppm and coupling constants (*J*) were reported in Hz. High-resolution mass spectra (HRMS) were performed on an electron spray injection (ESI) ThermoFisher Scientific LTQ FTICR mass spectrometer. High performance liquid chromatography (HPLC) analysis was performed at room temperature using a Diamonsil C18 (250 mm × 4.6 mm). All images were mounted and observed with a LEICA TCS SP8 Confocal Microscope System. Flow cytometry analysis measured by a FACSCalibur flow cytometer (BD Biosciences, USA).

2.2. Synthetic procedures for compounds 5-9

The route used for the synthesis of compound **9** is shown in Scheme 1, starting from commercially available 4-bromo-1,8-naphthalic anhydride **4**. Compound **4** was reacted with n-butylamine at reflux in ethanol to generate compound **5** [42,43], which subsequently underwent a palladium-catalyzed Suzuki cross-coupling reaction with 2-thienylboronic acid to afford compound **6** in acceptable yield. Compound **7** was achieved by bromination of compound **6** with Br_2 at a moderate condition, which was further converted to compound **8** by a palladium-catalyzed Suzuki cross-coupling reaction with 4-methoxyphenylboronicacid with a 58% yield. Finally, target compound **9** was afforded by demethylation of compound **8** with BBr_3 under N_2 with a relatively high yield of 42%. All the intermediates and the final product were carefully purified by column chromatography fully characterized by ^1H NMR, ^{13}C NMR and HR-MS spectroscopy (Supporting information).

2.2.1. Synthesis of 6-bromo-2-butyl-1H-benzo[de]isoquinoline-1,3(2H)-dione (5)

Compound **4** (5 g, 18 mmol), *n*-butylamine (1.6 g, 22 mmol) and anhydrous ethanol (40 mL) were added into a single-neck round-bottom flask connected with a condenser. The reaction mixture was heated to reflux overnight until the color of the solution became dark, and then cooled to precipitate. The resulting suspension was filtered and washed with cold ethanol twice to obtain the crude product. The crude material was purified by column chromatography on silica gel to obtain pale yellow solid **5** [42,43] (4.6 g), 76.7% yield, m.p. 106–108 °C. ^1H NMR (400 MHz, DMSO-d_6) δ 8.52 (dt, J = 12.9, 5.5 Hz, 2H), 8.30 (t, J = 6.1 Hz, 1H), 8.19 (t, J = 6.2 Hz, 1H), 7.97 (q, J = 7.0 Hz, 1H), 4.02 (q, J = 6.5 Hz, 2H), 1.61 (q, J = 7.0 Hz, 2H), 1.35 (p, J = 6.9 Hz, 2H), 0.93 (q, J = 6.6 Hz, 3H). ^{13}C NMR (101 MHz, DMSO-d_6) δ 163.28, 133.05, 132.03, 131.82, 131.42, 130.25, 129.55, 129.28, 128.76, 123.24, 122.46, 30.03,

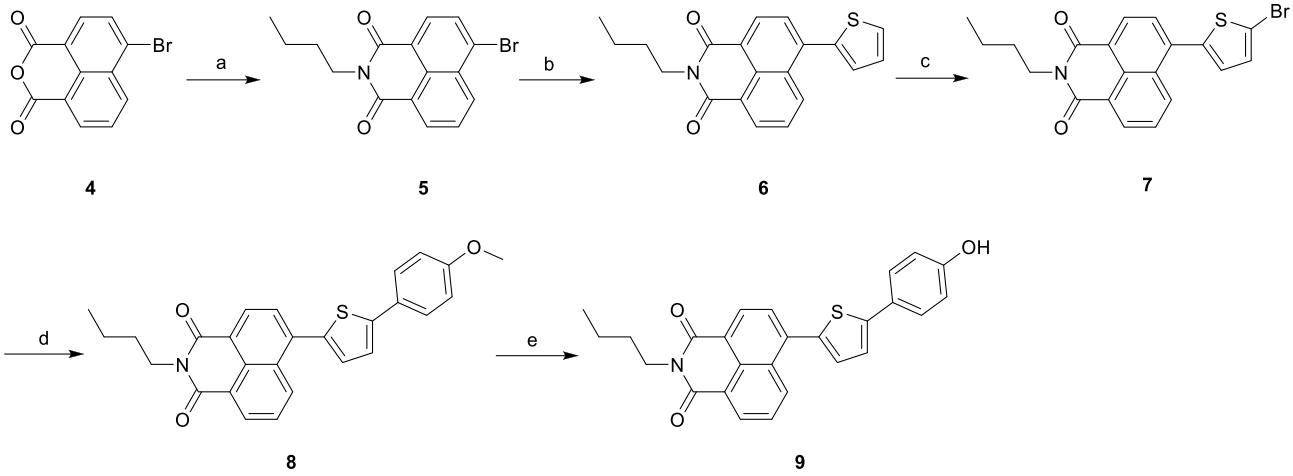

Scheme 1. Reagents and conditions: (a) n-butylamine, EtOH, reflux, 76.7%; (b) 2-thienylboronic acid, $Pd_2(dba)_3$, P(o-tol)$_3$, K_2CO_3, $(CH_3)_4NCl$, toluene/distilled water, 80 °C, 50.5%; (c) liquid Br_2, HOAc, RT, 73.3%; (d) 4-methoxyphenylboronicacid, $Pd_2(dba)_3$, P(o-tol)$_3$, K_2CO_3, $(CH_3)_4NCl$, toluene/distilled water, 80 °C, 57.8%; (e) BBr_3, DCM, N_2, RT, 41.7%.

20.27, 14.19. FT-IR (KBr, *v*, cm^{-1}): 3231, 3072, 2957, 2871, 2155, 1699, 1655, 1360, 1231. HR-MS (*m/z*) (ESI): calcd for $C_{16}H_{14}BrNO_2$ $[M + H]^+$: 332.0286, found: 332.0285.

2.2.2. Synthesis of 2-butyl-6-(thiophen-2-yl)-1H-benzo[de]isoquinoline-1,3(2H)-dione **(6)**

Under nitrogen protection, compound **5** (300 mg, 0.90 mmol), 2-thienylboronic acid (127 mg, 0.99 mmol), K_2CO_3 (997 mg, 7.2 mmol), $Pd_2(dba)_3$ (16.5 mg, 18 μmol), P(o-tol)$_3$ (22.0 mg, 72 μmol) and $(CH_3)_4NCl$ (10 mg, 90 μmol) were added into a three-neck round-bottom flask. After the mixture was degassed for 30 min, toluene (10 mL) and distilled water (2 mL) were added. The reaction contents were subsequently heated at 80 °C for 24 h. The resulting mixture was extracted with dichloromethane and washed with brine and distilled water. The organic extract was dried over sodium sulfate and collected under reduced pressure. The crude material was purified through column chromatography on silica to obtain **6** as a yellow solid (153 mg), 50.5% yield, m.p. 134–136 °C. ^{1}H NMR (400 MHz, $CDCl_3$) δ 8.57–8.46 (m, 3H), 7.75–7.68 (m, 1H), 7.68–7.61 (m, 1H), 7.46 (dd, *J* = 5.1, 0.8 Hz, 1H), 7.29–7.22 (m, 1H), 7.16 (ddd, *J* = 5.1, 1.8, 0.8 Hz, 1H), 4.11 (dd, *J* = 10.7, 4.2 Hz, 2H), 1.70–1.59 (m, 2H), 1.37 (dd, *J* = 15.0, 7.5 Hz, 2H), 0.90 (t, *J* = 7.4 Hz, 3H). ^{13}C NMR (100 MHz, $CDCl_3$) δ 164.16, 163.90, 139.77, 139.02, 132.25, 131.30, 130.60, 129.93, 128.89, 128.60, 127.93, 127.62, 127.15, 126.90, 122.93, 121.94, 77.33, 77.07, 76.75, 40.30, 30.21, 20.42, 13.89. FT-IR (KBr, *v*, cm^{-1}): 3450, 2960, 2930, 1697, 1658, 1610, 1592, 1390, 1291, 781. HR-MS (*m/z*) (ESI): calcd for $C_{20}H_{18}NO_2S$ $[M + H]^+$: 336.0980; found 336.1008.

2.2.3. Synthesis of 6-(5-bromothiophen-2-yl)-2-butyl-1H-benzo[de]isoquinoline-1,3(2H)-dione **(7)**

Compound **6** (70 mg, 0.21 mmol) and acetic acid (3 mL) were charged with a single-neck round-bottom flask under ambient conditions. After the compound was completely dissolved, liquid bromine (Br_2) (40 mg, 0.25 mmol) in dichloromethane (1 mL) was added. The reaction was kept stirring at room temperature for 1 h. Then the reaction mixture was extracted with dichloromethane and washed with saturated $NaHCO_3$ solution and brine. The organic extract was dried over sodium sulfate and collected under reduced pressure. The crude material was purified by column chromatography on silica gel to obtain pale yellow solid **7** (63 mg), 73.3% yield, m.p. 162–164 °C. ^{1}H NMR (400 MHz, $CDCl_3$) δ 8.61 (dd, *J* = 7.3, 1.0 Hz, 1H), 8.59–8.53 (m, 2H), 7.75 (dd, *J* = 9.4, 7.5 Hz, 2H), 7.20 (d, *J* = 3.8 Hz, 1H), 7.09 (d, *J* = 3.8 Hz, 1H), 4.22–4.13 (m, 2H), 1.77–1.67 (m, 2H), 1.51–1.40 (m, 2H), 0.98 (t, *J* = 7.4 Hz, 3H). ^{13}C NMR (100 MHz, $CDCl_3$) δ 164.05, 163.78, 141.25, 137.80, 131.79, 131.44, 130.76, 130.55, 129.77, 129.14, 128.65, 127.41, 123.04, 122.39, 114.46, 40.34, 30.20, 20.40, 13.88. FT-IR (KBr, *v*, cm^{-1}): 3450, 2963, 2931, 1698, 1655, 1613, 1590, 1388, 1231, 784. HR-MS (*m/z*) (ESI): calcd for $C_{20}H_{17}BrNO_2S$ $[M + H]^+$: 414.1185; found 414.1170.

2.2.4. Synthesis of 2-butyl-6-(5-(4-methoxyphenyl)thiophen-2-yl)-1H-benzo[de]isoquinoline-1,3(2H)-dione **(8)**

Under nitrogen protection, compound **7** (60 mg, 0.14 mmol), 4-methoxyphenylboronic acid (25 mg, 0.16 mmol), K_2CO_3 (160 mg, 1.1 mmol), $Pd_2(dba)_3$ (2.6 mg, 3 μmol), P(o-tol)$_3$ (3.5 mg, 10 μmol) and $(CH_3)_4NCl$ (1.6 mg, 14 μmol) were added into a three-neck round-bottom flask. After the mixture was degassed for 30 min, toluene (5 mL) and distilled water (1 mL) were added. The reaction contents were subsequently heated at 80 °C for 24 h. The resulting mixture was extracted with dichloromethane and washed with brine and distilled water. The organic extract was dried over sodium sulfate and collected under reduced pressure. The crude material was purified through column chromatography on silica to obtain **8** as a yellow solid (37 mg), 57.8% yield, m.p. 158–160 °C. ^{1}H NMR (400 MHz, $CDCl_3$) δ 8.71 (dd, *J* = 8.5, 0.9 Hz, 1H), 8.63 (dd, *J* = 7.2, 0.9 Hz, 1H), 8.58 (d, *J* = 7.6 Hz, 1H), 7.82 (d, *J* = 7.6 Hz, 1H), 7.75 (dd, *J* = 8.5, 7.3 Hz, 1H), 7.63–7.55 (m, 2H), 7.31 (d, *J* = 3.7 Hz, 1H), 7.29 (d, *J* = 3.7 Hz, 1H), 6.98–6.95 (m, 1H), 6.95–6.92 (m, 1H), 4.24–4.15 (m, 2H), 3.86 (s, 3H), 1.73 (tt, *J* = 7.7, 6.6 Hz, 2H), 1.46 (dd, *J* = 15.1, 7.5 Hz, 2H), 0.99 (t, *J* = 7.4 Hz, 3H). ^{13}C NMR (100 MHz, $CDCl_3$) δ 164.20, 163.93, 159.71, 146.85, 139.04, 137.96, 132.30, 131.33, 130.70, 129.95, 129.72, 128.90, 128.20, 127.14, 126.49, 122.93, 121.68, 114.48, 55.42, 40.31, 30.23, 20.43, 13.90. FT-IR (KBr, *v*, cm^{-1}): 3459, 2961, 1697, 1656, 1585, 1359, 1252, 1236, 1182, 781. HR-MS (*m/z*) (ESI): calcd for $C_{27}H_{24}NO_3S$ $[M + H]^+$: 442.1399; found 442.1388.

2.2.5. Synthesis of 2-butyl-6-(5-(4-hydroxyphenyl)thiophen-2-yl)-1H-benzo[de]isoquinoline-1,3(2H)-dione **(9)**

Compound **8** (50 mg, 0.11 mmol) was dissolved in dry CH_2Cl_2 (3 mL) and the solution was cooled to 0 °C by an ice bath. A solution of BBr_3 (569 mg, 2.3 mmol) in CH_2Cl_2 (2 mL) was added dropwise to the cold solution using a syringe. After the addition was completed, the stirring was continued for 1 h at 0 °C and then at rt. After the reaction was completed, the mixture was poured onto ice and was extracted with dichloromethane. The organic layer was washed with saturated $NaHCO_3$ solution and brine and dried over sodium sulfate. The crude material was purified by column chromatography on silica gel to obtain red solid **9** (20 mg), 41.7% yield, m.p. 149–151 °C. ^{1}H NMR (400 MHz, DMSO-d_6) δ 9.81 (s, 1H), 8.67 (d, *J* = 8.5 Hz, 1H), 8.47 (d, *J* = 7.1 Hz, 1H), 8.40 (d, *J* = 7.7 Hz, 1H), 7.85 (dt, *J* = 8.1, 4.0 Hz, 2H), 7.56 (d, *J* = 8.5 Hz, 2H), 7.49 (d, *J* = 3.7 Hz, 1H), 7.43 (d, *J* = 3.7 Hz, 1H), 6.86 (d, *J* = 8.5 Hz, 2H), 4.01 (t, *J* = 7.4 Hz, 2H), 1.68–1.55 (m, 2H), 1.36 (dd, *J* = 14.8, 7.4 Hz, 2H), 0.94 (t, *J* = 7.3 Hz, 3H). ^{13}C NMR (100 MHz, DMSO-d_6) δ 163.15, 162.84, 157.79, 146.50, 137.96, 136.37, 131.78, 130.74, 130.21, 128.56, 127.97, 127.61, 126.91, 124.14, 122.97, 122.32, 120.88, 115.93, 29.56, 19.78, 13.68. FT-IR (KBr, *v*, cm^{-1}): 3257, 2959, 1688, 1637, 1607, 1583, 1444, 1354, 1276, 1236, 1172, 780. HR-MS (*m/z*) (ESI): calcd for $C_{26}H_{22}NO_3S$ $[M + H]^+$: 428.1320; found 428.1318.

2.3. Quantum yields

Absorption spectra were recorded on a Varian Cary 100 spectrometer. Fluorescence spectra were measured with a Hitachi F-4500 fluorescence spectrometer with slit widths routinely set at 2.5 nm. Quantum yields (Φ) were determined relative to Rhodamine 6G (Q = 0.95, excitation = 440 nm) [51] and calculated according to the following formula:

$$\Phi_u = \Phi_s \times \frac{Fu}{Fs} \times \frac{Au}{As} \quad (3)$$

Φ_s equals the fluorescence quantum yield of the standard, typically taken from the literature; F presents the integrated spectral fluorescence photon flux at the detector and A presents the absorbance at the maximum excitation [52].

2.3.1. Cell culture

Human adenocarcinoma A549 cells, human breast carcinoma MCF-7 cells, human ovarian carcinoma SKOV-3 cells, and human colorectal adenocarcinoma HT-29 cells were purchased from the cell bank of the Chinese Academy of Sciences (Shanghai, China). A549 cells were cultured in F12 media. MCF-7 cells and SKOV-3 cells were cultured in DMEM media. HT-29 cells were cultured in McCoy's 5A medium. All media were supplemented with 10% (v/v) fetal bovine serum (FBS) and 1% (v/v) penicillin/streptomycin. Cells were incubated in a humid atmosphere of 5% CO_2 at 37 °C.

2.4. In vitro cellular uptake

For the purpose of observing the cellular uptake behavior of compound **9**, cells were plated in 20 mm glass-bottomed culture dishes at

proper densities and incubated for 24 h. Afterwards, different concentrations of compound **9** solution were equally added to the above cells and the mixture was incubated for different times. The cells were washed with PBS and stained with 4% paraformaldehyde and subsequently imaged using a Leica TCS SP8 confocal fluorescence microscope (Germany).

2.5. Flow cytometry analysis

To quantitatively analyze time-dependent cellular uptake, flow cytometry was performed to detect the fluorescence intensity of compound **9** inside the cells. Cells were grown in 6-well plates at proper densities and incubated for 24 h. Afterwards, 0.4 μM of compound **9** solution was added to the above cells for another 1, 2, 4 and 6 h. Then, the cells were trypsinized, washed three times with PBS along with centrifugation of 1300×*g* for 5 min, resuspended in 0.5 mL PBS and measured by a FACSCalibur flow cytometer (BD Biosciences, USA).

To quantitatively analyze concentration-dependent cellular uptake, flow cytometry was performed to detect the fluorescence intensity of compound **9** inside the cells. Cells were grown in 6-well plates at proper densities and incubated for 24 h. Afterwards, 0.1 μM, 0.2 μM, 0.4 μM and 1.0 μM **9** solution were added to the above cells for another 6 h. Then, the cells were trypsinized, washed three times with PBS along with centrifugation of 1300×*g* for 5 min, resuspended in 0.5 mL PBS and measured by FACSCalibur flow cytometry (BD Biosciences, USA).

2.6. Fluorescence lifetime measurements

All fluorescence lifetime measurements in solvents presented herein were performed using a F-7000 fluorescence spectrometer (Hitachi, Japan) coupling a pulsed diode laser. The mean-weighted fluorescence lifetime was calculated from both lifetime components (τ_i) and their amplitudes (α) using the equation [45]:

$$\tau = (\tau_1^2\alpha_1 + \tau_2^2\alpha_2)/ (\tau_1\alpha_1 + \tau_2\alpha_2) \quad (1)$$

2.7. Animal studies

Female BALB/c nude mice used for all *in vivo* studies were obtained from the Shanghai Institute of Material Medica, Chinese Academy of Sciences. The mice were housed and maintained under specific-pathogen-free conditions with access to enough sterile diet and water. All experimental procedures with animals were performed in accordance with the guidelines approved by the Institutional Animal Care and Use Committee at East China Normal University. MCF-7 cells (5×10^6) were subcutaneously injected into the right flank of the host mice and orthotopically xenografted to the nude mice.

2.8. CLSM imaging of MCF-7 nude mice tumor sections

At 6 h after the first injection of compound **9** (15 mg kg^{-1}), the mice (n = 3) with proper average tumor sizes (8.78 mm × 6.73 mm) and weights (17.5 g) were sacrificed by CO_2 inhalation, the tumors were excised, embedded in paraffin and sectioned into slices at a thickness of 8 μm for further CLSM imaging.

3. Results and discussion

3.1. Optical properties studies of compound 9

The optical properties of compound **9** were investigated in various solvents with different polarities. Table 1 shows the absorption, excitation and emission maxima and Stokes shift of **9** in different solvents. The absorption and emission spectra at a concentration of 1 μM for **9** in different solvents are also represented in Fig. 2A–B.

Table 1
Photophysical data of 9 in different solvents.

solvent	$E_T(30)$[a]	λ_{abs} (nm)[b]	λ_{ex} (nm)[c]	λ_{em} (nm)[d]	$\Delta\nu$ (cm^{-1})[e]	Φ[f]
H_2O	63.1	455	498	598	5255	0.041
EtOH	51.9	423	441	575	6249	0.032
CH_3CN	45.6	410	435	578	6339	0.034
DMSO	45.1	425	461	596	6750	0.032
DCM	40.7	415	437	566	6428	0.453
$CHCl_3$	39.1	420	442	567	6253	0.507
EA	38.1	410	436	560	6533	0.623
Cyclohexane	30.9	415	438	521	4902	0.160

[a] Solvent polarity parameter.
[b] Absorption maxima.
[c] Excitation maxima.
[d] Emission maxima.
[e] Stokes shift, $\Delta\nu$, were calculated using equation (1)/λ_{abs}-1/λ_{em}.
[f] Quantum yield.

Compound **9** is a typical donor-acceptor (D-A) type fluorophore with two absorption maxima and a large Stokes shift. The small absorption maxima are in the range of 310–330 nm which is characteristic of aromatic π-π* electron transition. The strong maxima in H_2O is at 455 nm, while the maxima in the other solvents were found in the range 410–425 nm (Fig. 2A and Table 1), centered at approximately 415 nm, arising from intramolecular charge transfer. In addition, the absorption spectra of compound **9** showed a redshift as with the increase of solvent polarity due to π conjugation. A large difference in the peak position of absorption and excitation spectra was observed, which was mainly due to intramolecular charge transfer in the excited state. As shown in Fig. 2B, compound **9** displayed positive solvatochromism of its emission and its emission maxima shifted to red when the solvent changed from cyclohexane to H_2O or DMSO. In the solvents more polar than acetonitrile, this long-wavelength emission was quenched, because the ICT state is known to be able to go through nonradiative deactivation in polar solvents. Quantum yields were observed an increase in cyclohexane, DCM, $CHCl_3$, and EA, from 0.160 to 0.623. The main cause is the stabilization of the twisted intramolecular charge-transfer (TICT) state due to strong solvation in a more polar medium. This leads to an increase in quantum yields [34]. However, much lower quantum yields were observed in higher polar solvents such as H_2O and alcohol. Higher solvation in polar solvents especially hydrogen bonding in water and alcohol results in the effective transformation of excitation energy into multiple vibrational quanta, which in contrast would decrease the values of the quantum yields.

3.2. Viscosity sensitivity studies of compound 9

As shown in Fig. 3, the normalized emission behaviors of compound **9** at varying viscosities were observed. Polyethylene glycol 400 (PEG-400) was used as a viscous solvent. The eleven mixtures of different viscosities, ranging from 0% to 100% PEG-400 (V/V) with pure ethanol, were used to determine the emission spectra of compound **9**.

The emission intensity spectra of compound **9** were also obtained in a mixed solution in EtOH with the percentage of PEG-400 increasing from 0% to 100% and the concentrations of **9** (1.0 μM) were kept low to reduce the possibility of forming hydrogen bonding, aggregation and self-quenching [46]. The enhancement of fluorescence was observed as the percentage of PEG-400 increased (Fig. 4). The result showed an approximately 8-fold enhancement of the fluorescence of intensity for compound **9**, indicating the viscosity sensitivity. The polarity of the solvent is known to affect the emission intensity of the charge transfer class of molecules. So, the influence of the increasing polarity of the protic and polar solvent (EtOH and PEG400) need to be considered. As a measure of polarity, the polarity function of these mixtures was

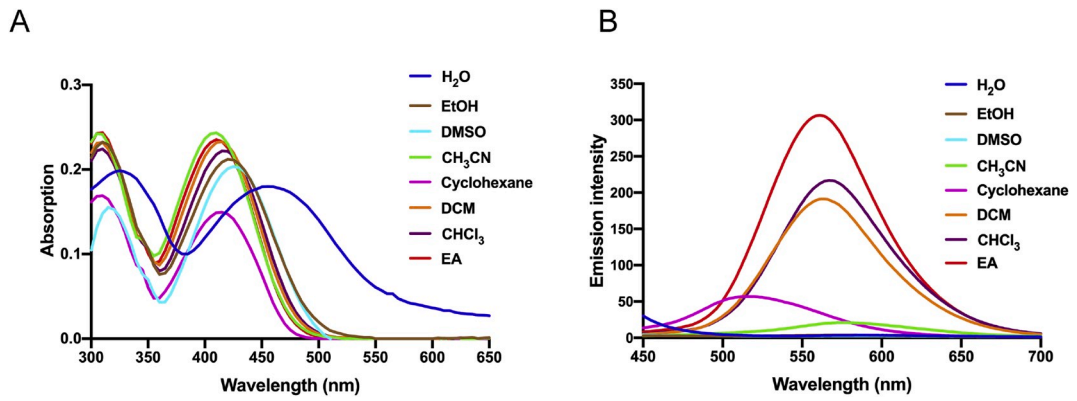

Fig. 2. (A) Absorption spectra of compound **9** in different solvents. (B) Corrected fluorescence emission spectra of compound **9** in different solvents. Excited at maximum excitation.

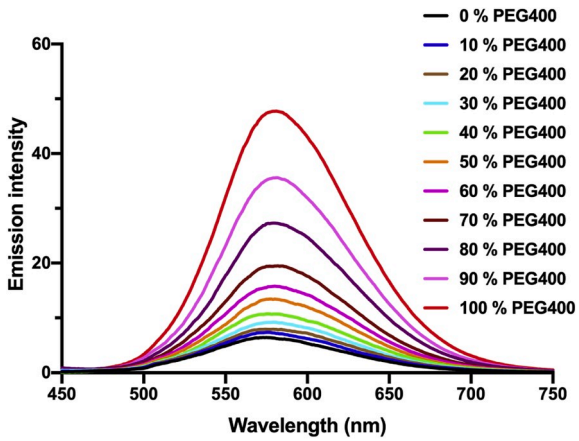

Fig. 3. Corrected fluorescence emission spectra of **9** in EtOH-PEG400 mixtures with different ratios. Excited at the maximum excitation.

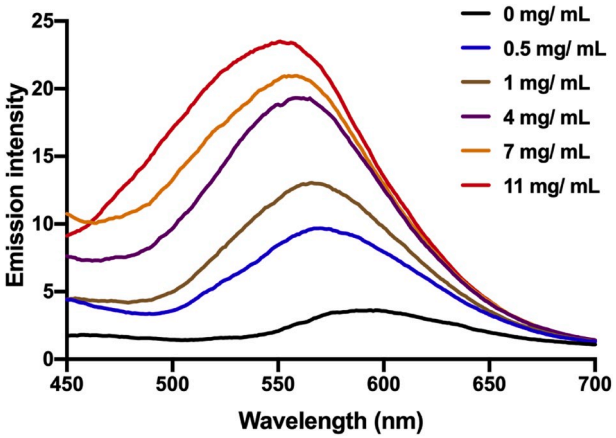

Fig. 4. Corrected fluorescence emission spectra of **9** in PBS with increasing concentrations of bovine serum albumin (BSA). Excited at the maximum excitation.

calculated. As reported, the polarity function stays constant at approximately 0.45 in EtOH-PEG400 mixtures [47,48], which indicated that the polarity of the mixtures would display a weak effect on emission intensity.

The fluorescence emission intensity of compound **9** and the effect of the viscosity of the solvent was described by using the Forster-Hoffmann equation (Eq. (2)) [44], and UV/Vis was used as the fluorescence emission spectra, where I is the emission intensity of the rotors, C is an empirical proportionality constant, x is the viscosity sensitivity and η is the viscosity of the solvent.

$$\log I = C + x \log \eta \quad (2)$$

The viscosity sensitivity (x), regression coefficient (R^2) and intercept (C) values and plot graph for compound **9** are shown in Fig. S1 and Table 2. The dependence of the emission intensity and solvent viscosity of compound **9** shows a relatively high exponent (x) value of 0.55 (R^2 = 0.9352). These outcomes elucidate that compound **9** has viscosity sensitivity, which is a typical characteristic of fluorescent molecular rotors.

3.3. Bovine serum albumin (BSA) sensitivity studies of compound 9

According to previous research, compound **9** possesses superior environmental sensitivity. To further evaluate this property, different concentrations of bovine serum albumin (BSA), ranging from 0 to 11 mg/mL were added to compound **9** in PBS. As shown in Fig. 4, the addition of BSA to compound **9** in PBS elicits a significant increase in fluorescence intensity and a blue shift in the emission maxima. Quantitatively, the fluorescence emission intensity of the 11 mg/mL BSA group was approximately 8-fold stronger than that of the blank group, which indicated that compound **9** showed the environmentally sensitive property.

3.4. Fluorescence lifetime measurements of compound 9

The molecular rotor properties are mainly governed by the excited state bond twisting or rotation, leading to non-radiative decay from the excited state back to the ground state. Thus, we performed fluorescence lifetime measurements of compound **9** in different solvents. The mean-weighted fluorescence lifetime was calculated from both lifetime components (τ_i) and their amplitudes (α) using the equation [45]:

$$\tau = (\tau_1^2\alpha_1 + \tau_2^2\alpha_2)/ (\tau_1\alpha_1 + \tau_2\alpha_2) \quad (4)$$

First, fluorescence decays measured for compound **9** at different solvents are shown in Fig. 5A and B. As shown in Fig. 5A, fluorescence decays of compound **9** in DCM, $CHCl_3$, and EA, which exhibited strong emission intensity, were measured. An increase in the fluorescence lifetime was observed from 1.4 ns to 2.9 ns with the increase of solvent

Table 2
Fluorescence emission viscosity sensitivity chart for compound **9**.

Compound	Slope (x)	R^2	Intercept
9	0.55	0.9352	0.45

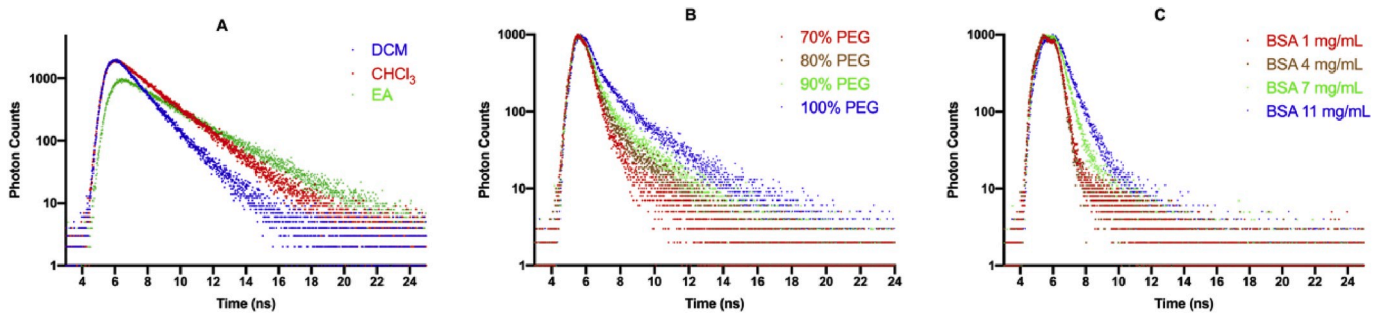

Fig. 5. The fluorescence decays of compound **9** in different solvents and BSA solution.

polarity. The main cause is the stabilization of the TICT state due to strong solvation in a more polar medium. This leads to an increase in lifetime and quantum yields (Table 1). However, fluorescence lifetime was below the limit of detection in higher polar solvents such as H_2O, DMSO, and alcohol due to the low emission intensity. Moreover, higher solvation in polar solvents especially hydrogen bonding in water and alcohol results in the effective transformation of excitation energy into multiple vibrational quanta, which in contrast would decrease the values of the fluorescence time.

Molecular rotors are fluorophores whose fluorescence lifetime increases with the increase of viscosity [49]. Viscous solvents are used to hinder the rotation of molecules, to block the TICT state. Fluorescence decays measured for compound **9** at increasing viscosity in EtOH-PEG400 mixtures are shown in Fig. 5B. The fluorescence lifetime was below the limit of detection in 0–60% PEG mixed solvents due to the low emission intensity. In addition, the fluorescence lifetime varies markedly with the increase of viscosity, increasing from 100 ps at 70% PEG400 to 1.8 ns at 100% PEG400, indicating the viscosity sensitivity of fluorescent molecular rotor.

We also studied fluorescence decays of compound 9 in the presence of different concentrations of BSA (Fig. 5B). As a trend, approximately an 8-fold increase in fluorescence lifetime of compound **9** was observed from 100 ps in 1 mg/mL BSA to 800 ps in 11 mg/mL BSA. This change was likely caused by the binding of the rotor **9** to a hydrophobic pocket of the protein, as was reported for other FMRs [50]. Deaggregation was also observed due to the addition of BSA (Fig. 4), which could lead to the enhancement in the emission yield. However, compared to emission intensity and fluorescence time, the effect of the addition of BSA was weaker than that of viscosity.

3.5. *In vitro time- and concentration-dependent cellular uptake of compound 9 in MCF-7 cells*

A functional example of the utility of environmental sensitivity was demonstrated in compound **9**'s application as a general cell stain in confocal imaging. To confirm whether compound **9** could be efficiently internalized into tumor cells and used for imaging of the tumor microenvironment, the *in vitro* cellular uptake behavior of compound **9** was investigated in tumor cell lines by confocal laser scanning microscopy (CLSM). To determine the relatively proper incubation time and concentration, time-dependent cellular uptake behavior was first investigated in MCF-7 cells. Cells with appropriate densities were treated with 0.4 μM of compound **9** at 37 °C for different times (1 h, 2 h, 4 h, and 6 h). As shown in Fig. 6, green fluorescence was observed in MCF-7 cells after incubation with compound **9** for 1 h, indicating the successful internalization of the rotor **9**. In addition, as the incubation time increased from 1 h to 6 h, the observed fluorescence inside the cells was greatly enhanced, indicating the time-dependent property of compound **9**. Based on the results, the concentration-dependent behavior of compound **9** was further evaluated. MCF-7 cells were incubated with compound **9** at different concentrations (0.1 μM, 0.2 μM, 0.4 μM and 1.0 μM) for 6 h. As shown in Fig. 7, green fluorescence was observed in all groups

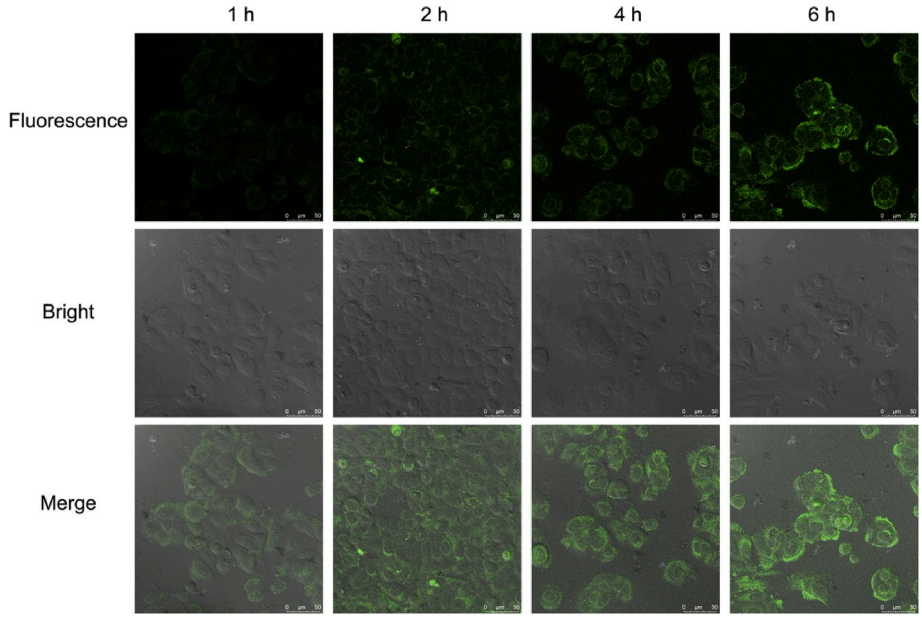

Fig. 6. Time-dependent cellular uptake behavior of compound **9** in MCF-7 cells. Cells were incubated with compound **9** at a concentration of 0.4 μM for different time (1 h, 2 h, 4 h and 6 h). (Scale bar = 50 μm).

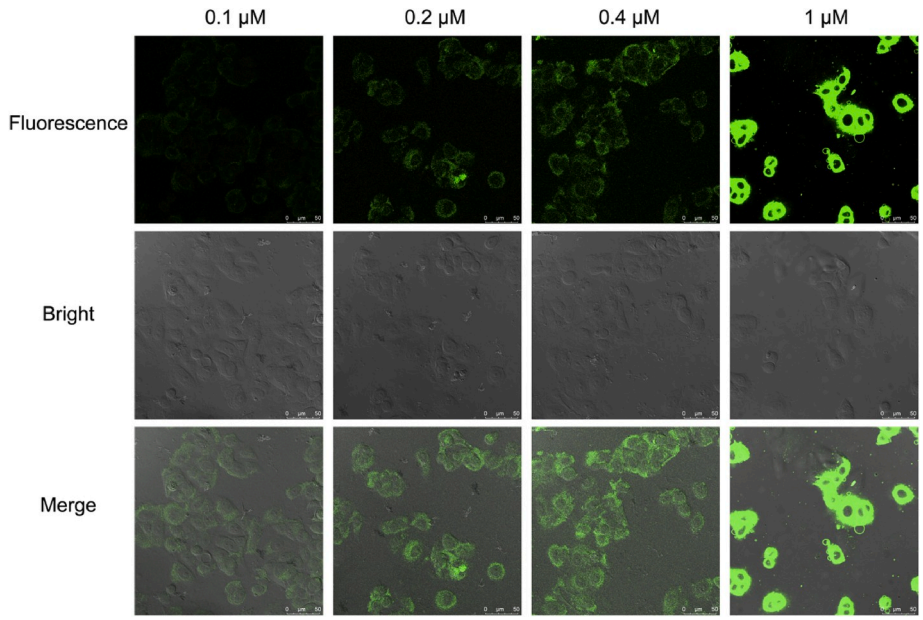

Fig. 7. Concentration dependent cellular uptake behavior of compound **9** in MCF-7 cells. MCF-7 cells were incubated with compound **9** at different concentrations (0.1 μM, 0.2 μM, 0.4 μM and 1.0 μM) for 6 h (Scale bar = 50 μm).

and when all groups were compared, a marked increase in the green emissions was seen as the concentration increased, also indicating the successful internalization.

3.6. Flow cytometry analysis

The quantitative analysis of cellular uptake was then examined by flow cytometry and the data also confirmed effective cellular uptake (Fig. 8). Notably, the mean fluorescence intensity (MFI) of compound **9** uptake in the 6 h group was approximately 3.2-fold stronger than that of the 1 h group, when MCF-7 cells were incubated with **9** for different times (1 h, 2 h, 4 h, and 6 h) at a concentration of 0.4 μM. Meanwhile, the MFI of compound **9** uptake in the 1.0 μM group was 5.5-fold stronger than that of the 0.1 μM group in the concentration-dependent experiment, which was consistent with previous *in vitro* CLSM cellular uptake assay results, further suggesting the time- and concentration-dependent properties of compound **9**.

3.7. In vitro cellular uptake of compound 9

Inspired by the previous results, compound **9** was used in three other cancer cell lines (A549 cells, HT-29 cells, and SKOV-3 cells) and MCF-7 cells for imaging by CLSM. Cells with appropriate densities were treated with 1 μM of compound **9** at 37 °C for 6 h. As shown in Fig. 9, when compound **9** was incubated with each of the four cell lines for 6 h, all groups were observed to have significant strong green fluorescence in the cytoplasm, suggesting the high cellular uptake and wide use in cancer cells. Cellular uptake behavior in normal HL7702 cells was also evaluated. As illustrated in Fig. 9, compound **9** showed almost negligible fluorescence in HL7702 cells, demonstrating lower cell internalization. Collectively, these differences between cancer cell lines and a normal cell line confirmed the cancer-specific properties of compound **9**.

3.8. CLSM assay of MCF-7 nude mice tumor sections

Encouraged by these results, sections from MCF-7 nude mice tumor tissues (treated for 6 h at 15 mg kg^{-1}) embedded in paraffin were also cut into a section of 8 μm for CLSM assay. As shown in Fig. 10, obvious fluorescence was observed in the tumor slides, suggesting the tumor imaging ability of **9**. These results are consistent with previous *in vitro* assay results, which further elucidates that **9** could be used for living cancer cell imaging and the visualization of tumor lesions with highly

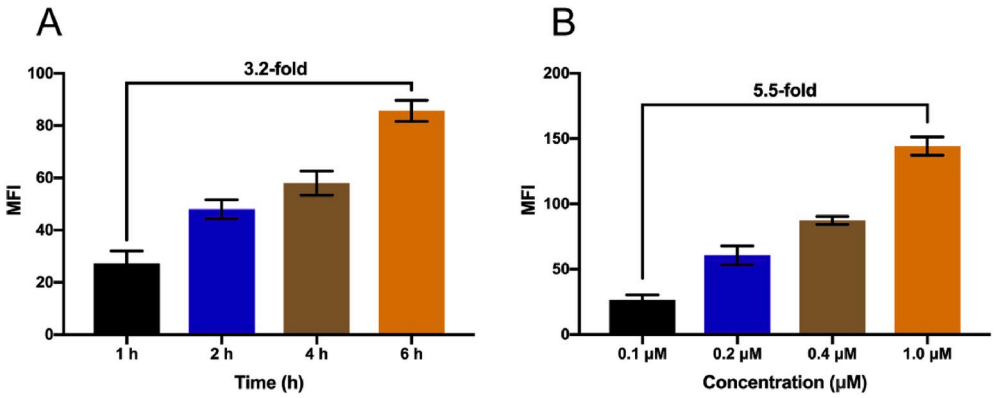

Fig. 8. Mean fluorescence intensity (MFI) of MCF-7 cells determined by flow cytometry analysis. (A) MCF-7 cells were incubated with compound **9** at a concentration of 0.4 μM for different times (1 h, 2 h, 4 h and 6 h). (B) MCF-7 cells were incubated with compound 9 at different concentrations (0.1 μM, 0.2 μM, 0.4 μM and 1.0 μM) for 6 h. The experiments were performed three times, and the results of the representative experiments are shown. Data were expressed as mean ± SD, n = 3.

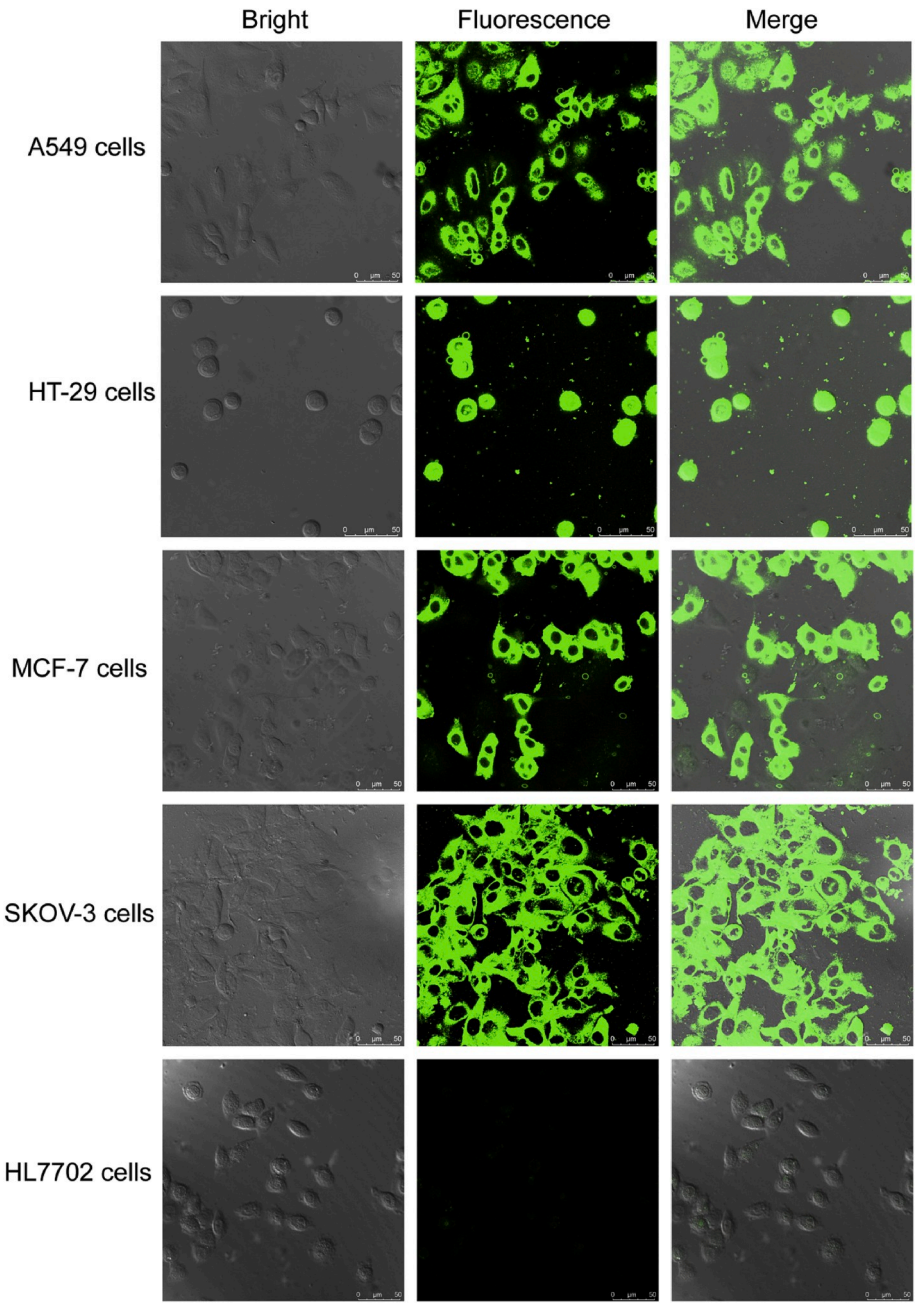

Fig. 9. *In vitro* cellular uptake of compound **9** in four cancer cell lines and one normal cell line. Cells were incubated with compound **9** at a concentration of 1.0 μM for 6 h.

effective tumor response.

4. Conclusion

In conclusion, a fluorescent viscosity sensor was established using a naphthalimide based fluorescent and low molecular rotor (**9**). Compound **9** exhibited favorable photophysical properties and high viscosity sensitivity in a glycerol-ethanol system which are typical properties of molecular rotors. Compound **9** also possessed high environmental sensitivity in that the addition of different concentrations of BSA to compound **9** in PBS elicited a significant 8-fold increase in fluorescence intensity. Fluorescence lifetime measurements further confirmed the viscosity and BSA sensitivity properties. Furthermore, compound **9** displayed obvious time-dependent and concentration-dependent cellular uptake behavior in MCF-7 cells and other tumor cell lines. *In vivo* CLSM assay of tumor sections from MCF-7 nude mice also confirmed the possibility of using compound **9** in tumor imaging. Overall, all these results elucidate that compound **9** could be used for imaging of the tumor micro-environment and the detection of cancer lesions. The hydroxyl group in compound **9** makes it easier to perform further structural optimization as probes for different factors, such as H_2O_2, hypochlorite, thiophenol, carbon monoxide and so on. In the future, it is possible that compound **9** could be conjugated to different high-affinity ligands for investigating various *in vivo* biochemical process increasing its range of applicability.

Declaration of competing interest

The authors declare that they have no known competing financial interests or personal relationships that could have appeared to influence

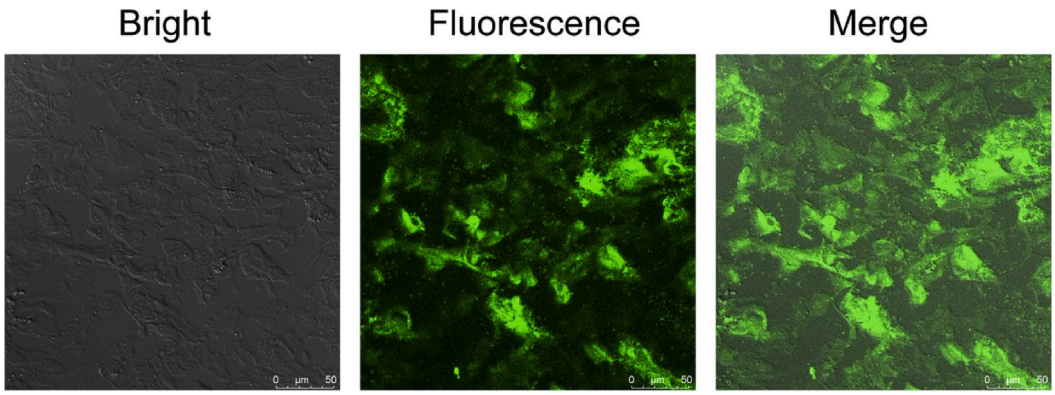

Fig. 10. Representative CLSM images of tumor sections from MCF-7 nude mice after treatment for 6 h with **9** (15 mg kg^{-1}). The experiments were performed three times, and the results of the representative experiments are shown. (Scale bar = 50 μm).

the work reported in this paper.

CRediT authorship contribution statement

Shulei Zhu: Conceptualization, Methodology, Writing - original draft. **Xumeng Yu:** Investigation, Formal analysis. **Yang He:** Investigation. **Mingliang Ma:** Validation. **Wei Lu:** Writing - review & editing, Supervision.

Acknowledgement

This work was supported by grants from the China Postdoctoral Science Foundation (Grant 2019M651435).

Appendix A. Supplementary data

Supplementary data to this article can be found online at https://doi.org/10.1016/j.dyepig.2020.108353.

References

[1] Yadav R, Yadav N, Kharya MD. A review: dye yielding sources and their importance. J Pharmacogn Phytochem 2014;6:241–8.
[2] Shahid M, Shahidul I, Mohammad F. Recent advancements in natural dye applications: a review. J Clean Prod 2013;53:310–31.
[3] Chen W, Dai Z, Liu H, Liu H, Shi Y, Li X. Photoinduced electron and energy transfer within a pyrene-perylenediimide dyad embedded in polymer matrixes. J Lumin 2015;168:192–8.
[4] Yuan L, Lin W, Yang Y, Chen H. A unique class of near-infrared functional fluorescent dyes with carboxylic-acid-modulated fluorescence ON/OFF switching: rational design, synthesis, optical properties, theoretical calculations, and applications for fluorescence imaging in living animals. J Am Chem Soc 2012;134:1200–11.
[5] Song L, Sun XD, Ge Y, Yao YH, Shen J, Zhang WB, Qian JH. A naphthalimide-based fluorescent probe for mercapto-containing compounds. Chin Chem Lett 2016;27:1776–80.
[6] Yang Z, Qin W, Lam JWY, Chen S, Sung HY, Williams ID, Tang BZ. Fluorescent pH sensor constructed from a heteroatom-containing luminogen with tunable AIE and ICT characteristics. Chem Sci 2013;4:3725–31.
[7] Georgiev NI, Bojinov VB, Nikolov PS. The design, synthesis and photophysical properties of two novel 1,8-naphthalimide fluorescent pH sensors based on PET and ICT. Dyes Pigments 2011;88:350–7.
[8] Zhang Y, Zhao Y, Wu Y, Zhao B, Wang L, Song B. Hemicyanine based naked-eye ratiometric fluorescent probe for monitoring lysosomal pH and its application. Spectrochim Acta A 2019:117767.
[9] Xu Y, Li B, Xiao L, Ouyang J, Sun S, Pang Y. A colorimetric and near-infrared fluorescent probe with high sensitivity and selectivity for acid phosphatase and inhibitor screening. Chem Commun 2014;50:8677–80.
[10] Guo B, Jing J, Nie L, Xin F, Gao C, Yang W, Zhang X. A lysosome targetable versatile fluorescent probe for imaging viscosity and peroxynitrite with different fluorescence signals in living cells. J Mater Chem B 2013;6:580–5.
[11] Hong Y, Lam JW, Tang BZ. Aggregation-induced emission: phenomenon, mechanism and applications. Chem. Commun. 2009;29:4332–53.
[12] Sheshashena RT, Shin SH, Choi MH. Effects of molecular flexibility/rigidity on the AIE/AIEE properties of aromatic thiols–substituted 1,8-naphthalimides. Dyes Pigments 2019;160:483–91.
[13] Ge SS, Li BY, Meng XL, Yan H, Yang M, Dong B, Lu Y. Aggregation-induced emission, multiple chromisms and selforganization of N-substituted-1,8-naphthalimides. Dyes Pigments 2018;148:147–53.
[14] Fu YX, Zhang JJ, Wang H, Chen JL, Zhao P, Chen GR, He XP. Intracellular pH sensing and targeted imaging of lysosome by a galactosyl naphthalimide-piperazine probe. Dyes Pigments 2016;133:372–9.
[15] Xu FY, Fan MY, Kang SS, Duan XR. A genetically encoded fluorescent biosensor for detecting nitroreductase activity in living cancer cells. Anal Chim Acta 2019;1088:131–6.
[16] Shinar J, Shinar R. Organic light-emitting devices (OLEDs) and OLED-based chemical and biological sensors: an overview. J Phys D 2008;41:133001.
[17] Ni Y, Hai Z, Zhang T, Wang Y, Yang Y, Zhang S, Liang G. Cathepsin B turning bioluminescence "on" for tumor imaging. Anal Chem 2019;91:14834–7.
[18] Lin Y, Ma Z, Li Z, Gao Y, Qin X, Zhang Z, Wang G, Du L, Li M. Bioluminescent probe for monitoring endogenous fibroblast activation protein-alpha. Anal Chem 2019;91:14873–8.
[19] Jacobson A, Petric A, Hogenkamp D, Sinur A, Barrio JR. 1,1-Dicyano-2-[6-(dimethylamino)naphthalen-2-yl]propene (ddnp): a solvent polarity and viscosity sensitive fluorophore for fluorescence microscopy. J Am Chem Soc 1996;118:5572–9.
[20] Er JC, Tang MK, Chia CG, Liew H, Vendrell M, Chang YT. MegaStokes BODIPY-triazoles as environmentally sensitive turn-on fluorescent dyes. Chem Sci 2013;4:2168–76.
[21] Cheng Y, Wang J, Qiu Z, Zheng X, Leung NLC, Lam JWY, Tang BZ. Multiscale humidity visualization by environmentally sensitive fluorescent molecular rotors. Adv Mater 2017;29:3900–6.
[22] Wang M, Zhang Y, Yue X, Yao S, Bondar MV, Belfield KD. A deoxyuridine-based far-red emitting viscosity sensor. Molecules 2016;21:709–20.
[23] Kudo K, Momotake A, Kanna Y, Nishimura Y, Arai T. Development of a quinoxaline-based fluorescent probe for quantitative estimation of protein binding site polarity. Chem. Commun. 2011;47:3867–9.
[24] Ghosh S, Jana S, Guchhait N. Domain specific association of small fluorescent probe trans-3-(4-monomethylaminophenyl)-acrylonitrile (MMAPA) with bovine serum albumin (BSA) and its dissociation from protein binding sites by Ag nanoparticles: spectroscopic and molecular docking study. J Phys Chem B 2012;116:1155–63.
[25] Haidekker MA, Brady TP, Lichlyter D, Theodorakis EA. Effects of solvent polarity and solvent viscosity on the fluorescent properties of molecular rotors and related probes. Bioorg Chem 2005;33:415–25.
[26] Weissig V. Targeted drug delivery to mammalian mitochondria in living cells. Expet Opin Drug Deliv 2005;2:89–102.
[27] Jadhav SD, Sekar N. Novel low-molecular weight styryl dyes based on 2-chloroimidazo[1,2-a]pyridine-3-carbaldehyde – synthesis and fluorescent molecular rotor studies. J Lumin 2017;190:289–97.
[28] Patil D, Jadhav M, Avhad K, Gawale Y, Sekar N. NIR emitting new N, N-diethylaniline based NLOphoric D-π-A and D-A′-π-A dyes: photophysical properties, viscosity sensitivity and DFT studies. J Lumin 2018;204:436–47.
[29] Avhad KC, Patil DS, Chitrambalam S, Sreenath MC, Joe IH, Sekar N. Viscosity induced emission of red-emitting NLOphoric coumarin morpholine-thiazole hybrid styryl dyes as FMRs: consolidated experimental and theoretical approach. Opt Mater 2018;79:90–107.
[30] Wu Z, Cui J, Qian X. Rational design of fluorescent viscosity sensors by the principle of photoinduced electron transfer. Tetrahedron Lett 2013;54:2575–8.
[31] Loutty RO, Law KY. Electrochemistry and spectroscopy of intramolecular charge-transfer complexes. p-/V,/V-Dlalkylamlnobenzylldenemalononitrlles. J Phys Chem 1980;84:2803–8.
[32] Haidekker MA, Brady TP, Chalian SH, Akers W, Lichlyter D, Theodorakis EA. Hydrophilic molecular rotor derivatives-synthesis and characterization. Bioorg Chem 2004;32:274–89.
[33] Jin RF, Tang SS, Sun WD. Rational design of donor-π-acceptor n-butyl-1,8-naphthalimide-cored branched molecules as charge transport and luminescent materials for organic light-emitting diodes. Tetrahedron 2014;70:47–53.

[34] Panchenko PA, Arkhipova AN, Fedorova OA, Fedorov YV, Zakharko MA, Arkhipov DE, Jonusauskas G. Controlling photophysics of styrylnaphthalimides through TICT, fluorescence and *E, Z*-photoisomerization interplay. Phys Chem Chem Phys 2017;19:1244–56.
[35] Lin HH, Chan YC, Chen JW, Chang CC. Aggregation-induced emission enhancement characteristics of naphthalimide derivatives and their applications in cell imaging. J Mater Chem 2011;21:3170–7.
[36] Lee J, Yoon SA, Chun J, Kang C, Lee MH. A red-emitting styrylnaphthalimide-based fluorescent probe providing a ratiometric signal change for the precise and quantitative detection of H_2O_2. Anal Chim Acta 2019;1080:153–61.
[37] Lee SC, Heo J, Woo HC, Lee JA, Seo YH, Lee CL, Kim S, Kwon OP. Fluorescent molecular rotors for viscosity sensors. Chem Eur J 2018;24:13706–18.
[38] Kuimova MK, Yahioglu G, Levitt JA, Suhling K. Molecular rotor measures viscosity of live cells via fluorescence lifetime imaging. J Am Chem Soc 2008;130:6672–3.
[39] Karpenko IA, Niko Y, Yakubovskyi VP, Gerasov AO, Bonnet D, Kovtun YP, Klymchenko AS. Push–pull dioxaborine as fluorescent molecular rotor: far-red fluorogenic probe for ligand–receptor interactions. J Mater Chem C 2016;4:3002–9.
[40] Peng X, Yang Z, Wang J, Fan J, He Y, Song F, Wang B, Sun S, Qu J, Qi J, Yan M. Fluorescence ratiometry and fluorescence lifetime imaging: using a single molecular sensor for dual mode imaging of cellular viscosity. J Am Chem Soc 2011;133:6626–35.
[41] Kuimova MK, Botchway SW, Parker AW, Balaz M, Collins HA, Anderson HL, Suhling K, Ogilby PR. Imaging intracellular viscosity of a single cell during photoinduced cell death. Nat Chem 2009;1:69–73.
[42] Cai YS, Guo ZQ, Chen JM, Li WL, Zhong LB, Gao Y, Jiang L, Chi LF, Tian H, Zhu WH. Enabling light work in helical self-assembly for dynamic amplification of chirality with photoreversibility. J Am Chem Soc 2016;138:2219–24.
[43] Nagarajan K, Gopan G, Cheriya RT, Hariharan M. Long alkyl side-chains impede exciton interaction in organic light harvesting crystals. Chem. Commun. 2017;53:7409–11.
[44] Förster T, Hoffmann GZ. Viscosity dependence of fluorescent quantum yields of some dye systems. Phys Chem 1971;75:63–76.
[45] Dent MR, López DI, Dickson CJ, Chairatana P, Anderson HL, Gould IR, Wylie D, Vysniauskas A, Brooks NJ, Kuimova MK. Imaging plasma membrane phase behaviour in live cells using a thiophene-based molecular rotor. Chem. Commun. 2016;52:13269–72.
[46] Levitt JA, Chung PH, Kuimova MK, Yahioglu G, Wang Y, Qu J, Suhling K. Fluorescence anisotropy of molecular rotors. ChemPhysChem 2011;12:662–72.
[47] Scholz N, Jadhav A, Shreykar M, Behnke T, Nirmalananthan N, Resch-Genger U, Sekar N. Coumarin-Rhodamine hybrids—novel probes for the optical measurement of viscosity and polarity. J Fluoresc 2017;27:1949–56.
[48] Seedher N, Bhatia S. Solubility enhancement of Cox-2 inhibitors using various solvent systems. AAPS PharmSciTech 2003;4:36–44.
[49] Haidekker MA, Theodorakis EA. Molecular rotors-fluorescent biosensors for viscosity and flow. Org Biomol Chem 2007;5:1669–78.
[50] Wu YY, Yu WT, Hou TC, Liu TK, Huang CL, Chen IC, Tan KT. A selective and sensitive fluorescent albumin probe for the determination of urinary albumin. Chem. Commun. 2014;50:11507–10.
[51] Kubin RF, Fletcher AN. Fluorescence quantum yields of some rhodamine dyes. J Lumin 1982;27:455–62.
[52] Würth C, Pauli J, Lochmann C, Spieles M, Resch GU. Integrating sphere setup for the traceable measurement of absolute photoluminescence quantum yields in the near infrared. Anal Chem 2012;84:1345–52.